



HAL
open science

Solution-State Spin Crossover in a Family of [Fe(L)₂(CH₃CN)₂](BF₄)₂ Complexes

Benjamin Wilson, Hayley Scott, Rosanna Archer, Corine Mathonière,
Rodolphe Clérac, Paul Kruger

► **To cite this version:**

Benjamin Wilson, Hayley Scott, Rosanna Archer, Corine Mathonière, Rodolphe Clérac, et al..
Solution-State Spin Crossover in a Family of [Fe(L)₂(CH₃CN)₂](BF₄)₂ Complexes. *Magnetochemistry*, 2019, 5 (2), 22 (13 p.). 10.3390/magnetochemistry5020022 . hal-02171591

HAL Id: hal-02171591

<https://hal.science/hal-02171591v1>






Submitted on 20 Jul 2020

HAL is a multi-disciplinary open access archive for the deposit and dissemination of scientific research documents, whether they are published or not. The documents may come from teaching and research institutions in France or abroad, or from public or private research centers.

L'archive ouverte pluridisciplinaire **HAL**, est destinée au dépôt et à la diffusion de documents scientifiques de niveau recherche, publiés ou non, émanant des établissements d'enseignement et de recherche français ou étrangers, des laboratoires publics ou privés.

Article

Solution-State Spin Crossover in a Family of $[\text{Fe}(\text{L})_2(\text{CH}_3\text{CN})_2](\text{BF}_4)_2$ Complexes

Benjamin H. Wilson ^{1,2,3} , Hayley S. Scott ^{1,*} , Rosanna J. Archer ¹, Corine Mathonière ^{4,5} , Rodolphe Clérac ^{2,3}  and Paul E. Kruger ^{1,*} 

¹ MacDiarmid Institute, School of Physical and Chemical Science, University of Canterbury, Private Bag 4800, Christchurch 8041, New Zealand; benjamin.wilson@pg.canterbury.ac.nz (B.H.W.); rosanna.archer@pg.canterbury.ac.nz (R.J.A.)

² CNRS, CRPP, UMR 5031, F-33600 Pessac, France; clerac@crpp-bordeaux.cnrs.fr

³ Univ. Bordeaux, CRPP, UMR 5031, F-33600 Pessac, France

⁴ CNRS, ICMCB, UMR 5026, F-33600 Pessac, France; Corine.Mathoniere@icmcb.cnrs.fr

⁵ Univ. Bordeaux, ICMCB, UMR 5026, F-33600 Pessac, France

* Correspondence: hayley.scott@canterbury.ac.nz (H.S.S.); paul.kruger@canterbury.ac.nz (P.E.K.)

Received: 19 January 2019; Accepted: 7 March 2019; Published: 1 April 2019



Abstract: We report herein on five new Fe(II) complexes of general formula $[\text{Fe}(\text{L})_2(\text{NCCH}_3)_2](\text{BF}_4)_2 \cdot x\text{CH}_3\text{CN}$ (L = substituted 2-pyridylimine-based ligands). The influence of proximally located electron withdrawing groups (e.g., NO_2 , CN , CF_3 , Cl , Br) bound to coordinated pyridylimine ligands has been studied for the effect on spin crossover in their Fe(II) complexes. Variable-temperature UV-visible spectroscopic studies performed on complexes with more strongly electronegative ligand substituents revealed spin crossover (SCO) in the solution, and thermodynamic parameters associated with the spin crossover were estimated.

Keywords: spin crossover; Fe(II); supramolecular chemistry; solution-state SCO; molecular magnetism; crystallography

1. Introduction

Spin crossover (SCO) [1–3] describes the phenomenon of spin state switching in some $3d^4$ – $3d^7$ transition metal complexes. Pursuits to create new variants are largely driven by a desire to better exploit the inherent switchability of these systems for application within molecular devices [4–6]. Octahedral Fe(II) complexes are the most widely studied, because the interconversion between the diamagnetic low-spin (LS) state ($S = 0$) and paramagnetic high-spin (HS) state ($S = 2$) is accompanied by striking associated changes in structural and optical properties [7,8]. Triggering SCO requires the application of an external stimulus, such as light, changes in temperature or pressure [9–12].

The presence and nature of SCO are related to two main features intrinsic to the compounds: (i) The electronic properties (including the ligand field strength); [13] and, (ii) cooperative supramolecular or covalent pathways between spin switching centres [14]. While optimisation and tuning of the ligand field may be achieved through modification of coordinated ligands [15–18], gaining precise control over the cooperativity and elastic intermolecular interactions is more difficult to achieve. The study of SCO in the solution state has therefore been offered as a means to investigate magnetic properties, whereby the intermolecular interactions found in the solid state are mitigated, allowing for rationalisation of the molecular magnetic character of the isolated complexes [19].

The primary aim of this work was to employ solution-state SCO studies in a wider investigation which targeted the tuning of the ligand field within a series of related Fe(II) complexes. Our work focused on the incorporation of bidentate 2-pyridylimine-based ligands into mononuclear Fe(II)

complexes. The strong ligand field supplied by the 2-pyridylimine moiety typically yields Fe(II) complexes in the LS state, making these complexes suited to ligand field “tuning” (via ligand functionalisation) in attempts to realise SCO [20,21].

Our strategy for optimising the ligand field followed from an approach employed previously in similar systems, whereby variation of electronegative substituents appended to ligands was used as a method to modify their electron-donating character and therefore the magnetic properties of their complexes [22–24]. Within this study, five new asymmetric ligands based upon the 2-pyridylimine motif were synthesised which contained electron-withdrawing substituents, varied at two ligand sites, “X” (with CF₃, CN and NO₂) and “Y” (with Cl and Br), producing the ligand series L1–L5 (see Figure 1).

We report herein the synthesis of five mononuclear Fe(II) compounds (1–5) of general formula *cis*-[Fe(L)₂(CH₃CN)₂](BF₄)₂•*x*CH₃CN. Compounds 1–5 have had their structures comprehensively characterised. Variable-temperature UV-visible spectroscopic analyses were performed on compounds 3–5 to probe the occurrence of solution-state SCO.

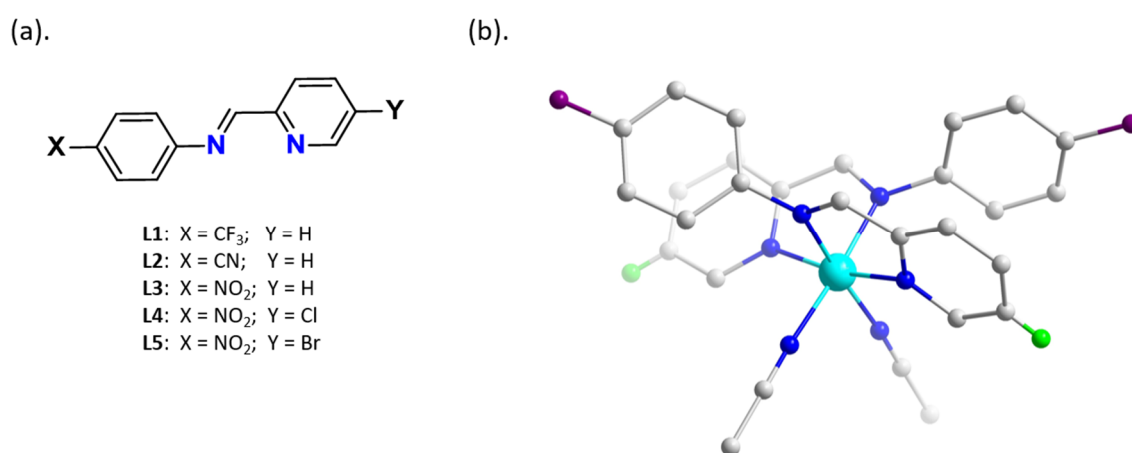


Figure 1. (a) Ligands L1–L5 incorporated into complexes 1–5. Coordinating N-donor atoms are coloured in blue. (b) Overall structural arrangement of complexes [Fe(L)₂(CH₃CN)₂]²⁺ (1–5). Atom colouring corresponds to: Cyan (Fe), grey (carbon), blue (nitrogen), purple (X: CF₃, CN, NO₂) and green (Y: H, Cl, Br). Anions, H-atoms and solvent molecules have been omitted for clarity.

2. Results

Ligands L1–L3 were prepared via reaction of 2-pyridinecarboxaldehyde and the corresponding aromatic amine. The ligand was then further reacted with Fe(BF₄)₂·6H₂O in acetonitrile to yield complexes 1–3, which crystallised following slow diffusion of diethyl ether into the mother liquor. Complexes 4 and 5 were formed in situ by reaction of p-nitroaniline, 5-R-2-pyridinecarboxaldehyde (R = Cl for L4 and complex 4, Br for L5 and complex 5) and Fe(BF₄)₂·6H₂O in acetonitrile. Filtration of the reaction mixture and diffusion of diethyl ether into the filtrate produced single crystals for analysis.

It should be noted that the formation of the tris-pyridylimine coordinated complex [25] was the initial target product for this study, however in acetonitrile solvent [Fe(L)₂(CH₃CN)₂] was the only product that was identified.

2.1. Single Crystal Structural Analysis

The coordination environment of complexes 1–5 share many similar features and so a general description of the overall structural conformation is given below, followed by a description of each complex, highlighting salient differences between structures.

Each of the complexes 1–5 crystallise in the monoclinic space group C2/c. They each consist of a monomeric Fe(II) complex bound to two bidentate 2-pyridylimine groups in a *cis* arrangement from two different ligands. The coordination of two CH₃CN molecules completes the coordination sphere,

binding through the nitrile N-atoms. For each complex, the Fe(II) centres sit on a two-fold rotation symmetry element and the asymmetric unit comprises half of each monomeric complex and a single BF_4^- anion (labelled asymmetric unit figures for complexes **1–5** are given in Figures S1–S5). A summary of structural data for compounds **1–5** is given in Table 1 and Tables S1–S3.

The structure of compound **1** was collected at 120 K, yielding Fe–N bond lengths in the range of 1.964(3) to 1.971(3) Å, suggestive of the LS state for Fe(II) centres. The pseudo-octahedral geometry of the Fe(II) centre sees a $\text{N}_{\text{im}}\text{-Fe-N}_{\text{pyr}}$ bite angle of $80.84(11)^\circ$ and a $\text{N}_{\text{NCCH}_3}\text{-Fe-N}_{\text{NCCH}_3}$ angle of $85.35(15)^\circ$. The octahedral distortion parameter, Σ [26], around Fe(II) centres is equal to 54.3° . There is significant torsional twisting within the **L1** ligands about the imine-phenyl plane, equal to 59.88° . This twisting of the phenyl ring causes it to lie face-to-face with the pyridyl ring of the second **L1** ligand, bound within the same mononuclear complex, producing centroid . . . centroid distances of 3.853 Å (Figure 2). Of particular interest is the lack of displacement of the aromatic rings relative to one another. Usually in face-to-face $\pi\text{-}\pi$ interactions ring “slippage” occurs where one ring shifts relative to the other to optimise the electrostatic interaction between the electron-rich π system and the electron-poor σ system (i.e., the hydrogen atoms). In compound **1**, both pyridine and benzotrifluoride aromatic systems are π -deficient and this has been observed to increase the stability of aligned face-to-face $\pi\text{-}\pi$ interactions. While interactions of this type are uncommon, there is precedence within the literature [27]. Several weak intermolecular interactions exist between complexes, $[\text{BF}_4]^-$ anions and acetonitrile solvent molecules, producing a series of weak intermolecular interactions, predominantly CH . . . F; these are listed in Tables S1–S4.

The structure of compound **2** was collected at 120 K. At this temperature, the Fe(II) centre is in a LS configuration with coordinating bond lengths ranging from 1.938(1) to 1.973(1) Å. The pseudo-octahedral geometry of the Fe(II) centre sees a $\text{N}_{\text{im}}\text{-Fe-N}_{\text{pyr}}$ bite angle of $81.06(6)^\circ$ and a $\text{N}_{\text{NCCH}_3}\text{-Fe-N}_{\text{NCCH}_3}$ angle of $85.08(6)^\circ$. The octahedral distortion parameter, Σ , is equal to 48.9° . As was the case for compound **1**, the **L2** ligands undergo significant distortion away from planarity about the imine-phenyl bond. The torsion angle of 61.0° produces a face-to-face $\pi\text{-}\pi$ interaction between the pyridyl and phenyl rings equal to 3.891 Å. There are several weak intermolecular interactions, or close contacts between complexes, $[\text{BF}_4]^-$ anions and acetonitrile solvent molecules; these are listed in Table S4.

The structure of compound **3** was collected at 293 K. At this temperature, the coordinating bond lengths about the Fe(II) centre range from 1.945(2) to 1.993(2) Å, consistent with Fe(II) in the LS state. The pseudo-octahedral geometry of the Fe(II) centre sees a $\text{N}_{\text{im}}\text{-Fe-N}_{\text{pyr}}$ bite angle of $80.06(8)^\circ$ and a $\text{N}_{\text{NCCH}_3}\text{-Fe-N}_{\text{NCCH}_3}$ angle of $89.2(9)^\circ$. The octahedral distortion parameter, Σ , is equal to 45.9° . The torsional twist of the imine-phenyl bond in **L3** is significant and equal to $71.2(3)^\circ$, producing face-to-face $\pi\text{-}\pi$ interactions between phenyl and pyridyl centroids equal to 3.684 Å. Intermolecular interactions between molecules can be attributed to non-classical hydrogen bonding between a polarised C–H bond situated on the pyridine group and the *p*- NO_2 substituents on adjacent complexes, with a donor–acceptor distance of 3.162 Å. This forms a 1D-hydrogen bonding network along the crystallographic (101) plane (see Figure 3). Further, weaker interactions between complexes and anions are listed in Table S4. There are no solvent molecules present in the second coordination sphere. Upon immersion of the crystals of compound **3** under a N_2 stream for low temperature structural analysis, degradation of crystallinity occurred. This behaviour is typically ascribed to a first order phase transition that has been reported to occur in compounds undergoing a SCO. As the crystallographic data show that the sample was in the LS state at room temperature, the phase transition could not be due to SCO. Attempts to measure unit cell parameters as the sample was cooled in 10 K increments from 240 K to 150 K were made, however visible loss of crystallinity and subsequent loss of diffraction occurred at ca. 220 K.

The structure of compound **4** was collected at 270 K. At this temperature, the coordinating bond lengths about the Fe(II) centre range from 1.946(4) to 1.972(3) Å, consistent with Fe(II) in the LS state. The pseudo-octahedral geometry of the Fe(II) centre sees a $\text{N}_{\text{im}}\text{-Fe-N}_{\text{pyr}}$ bite angle of $80.89(14)^\circ$ and a $\text{N}_{\text{NCCH}_3}\text{-Fe-N}_{\text{NCCH}_3}$ angle of $92.3(2)^\circ$. The octahedral distortion parameter, Σ , is equal to 50.6° . There

are no solvent molecules in the outer coordination sphere. Torsional twisting within **L4** about the imine-phenyl produces an angle equal to 69.69° , yielding a $\pi \dots \pi$ stacking distance of 3.966 \AA between the pyridyl and phenyl groups (centroid \dots centroid). Weak intermolecular interactions and close contacts are given in Table S4. Similar to compound **3**, the structure of compound **4** could only be collected at 270 K, as attempts to collect structural data at lower temperatures caused the crystals to shatter and lose crystallinity.

The structure of compound **5** was collected at 270 K. At this temperature, the coordinating bond lengths about the Fe(II) centre range from $1.947(3)$ to $1.984(3) \text{ \AA}$, consistent with Fe(II) in the LS state. The pseudo-octahedral geometry of the Fe(II) centre sees a $N_{\text{im}}\text{-Fe-}N_{\text{pyr}}$ bite angle of $81.04(12)^\circ$ and a $N_{\text{NCCH}_3}\text{-Fe-}N_{\text{NCCH}_3}$ angle of $91.09(18)^\circ$. The octahedral distortion parameter, Σ , is equal to 47.1° . There are no solvent molecules in the outer coordination sphere. Torsional twisting within **L5** about the imine-phenyl produces an angle equal to 70.83° , yielding a $\pi \dots \pi$ stacking distance of 3.970 \AA between the pyridyl and phenyl groups (centroid \dots centroid). Like analogues **3** and **4**, the structure of compound **5** could only be collected at 270 K, as attempts to collect structural data at lower temperatures caused the crystals to shatter and lose crystallinity.

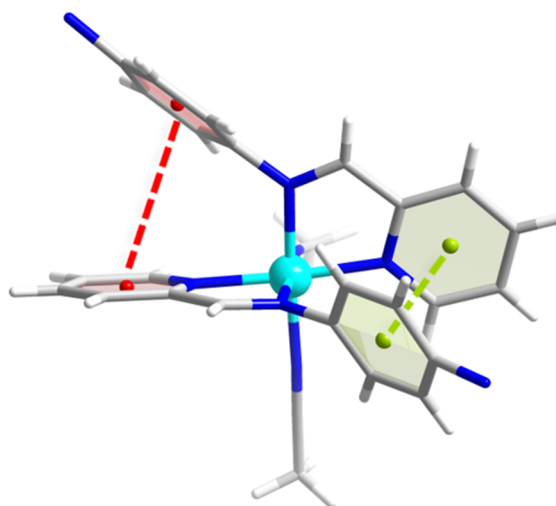


Figure 2. Face-to-face π - π stacking between pyridyl and phenyl groups of adjacent ligands in the series of complexes **1**-**5** (complex **2** depicted). Increased imine-phenyl torsional twisting produces shorter centroid \dots centroid distances.

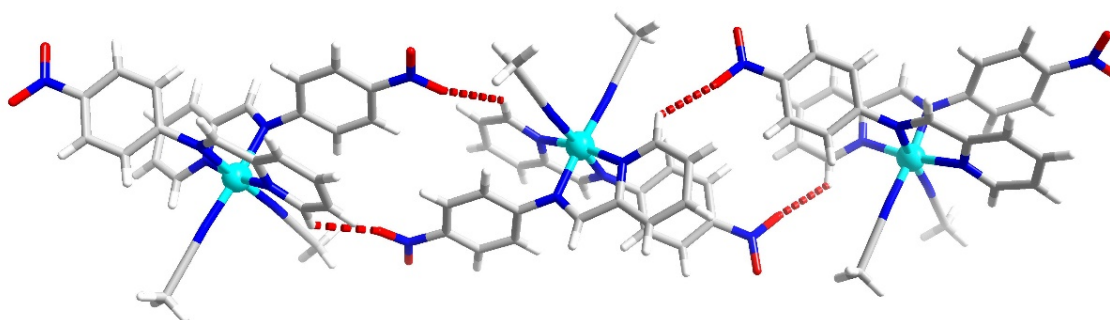


Figure 3. Intermolecular hydrogen bonding interactions ($\text{CH} \dots \text{O}$) in complex **3**, forming a 1-D supramolecular network in the crystallographic (101) plane.

Table 1. Summary of structural parameters for complexes 1–5.

	1	2	3	4	5
Space Group	<i>C2/c</i>	<i>C2/c</i>	<i>C2/c</i>	<i>C2/c</i>	<i>C2/c</i>
Formula	[Fe(L1) ₂ (CH ₃ CN) ₂] ₂ ·2CH ₃ CN	[Fe(L2) ₂ (CH ₃ CN) ₂] ₂ ·2CH ₃ CN	[Fe(L3) ₂ (CH ₃ CN) ₂]	[Fe(L4) ₂ (CH ₃ CN) ₂]	[Fe(L5) ₂ (CH ₃ CN) ₂]
T/K	120(2)	120(2)	293(2)	270(2)	270(2)
Crystal Colour	Purple	Purple	Black	Red	Red
Av. Fe–N Distance (Å)	1.95	1.96	1.98	1.96	1.96
Fe^{II} Spin State	LS	LS	LS	LS	LS
Σ (°)^a	54.3	48.9	45.9	50.69	47.15
cis N_{imine}–Fe–N_{pyridyl} (°)	80.84	81.06	80.06	80.89	81.04
Imine-phenyl torsion (°)	59.88	61.0	71.2	69.69	70.83

^a Derived from the N–Fe–N angles and is the sum of the deviations from 90° of the 12 *cis* N–Fe–N angles in the coordination sphere, Σ is equal to 0 for an ideal octahedron and increases with the deformation [26].

2.2. Variable-Temperature UV-Visible Spectroscopic Studies

Acetonitrile solutions of complexes 1–5 were prepared and were all deep purple-red in colour at room temperature. Solutions were heated to ca. 350 K at which temperature, the colour of complexes 3–5 changed from a raspberry red to pale peach colour, suggesting SCO may be occurring. Solutions of complexes 1 and 2 remained deep purple-red in colour over the temperature range measured, indicating retention of the LS state. Observation of a colour change in complexes 3–5 prompted us to probe the SCO characteristics of these complexes using variable-temperature UV-visible characterisations. Solutions of complexes 3–5 were prepared in acetonitrile, at concentrations 0.40 mmol L⁻¹ (3), 0.24 mmol L⁻¹ (4) and 0.25 mmol L⁻¹ (5). Samples were analysed over the temperature ranges 275 or 283–343 K, with 2 K increments between 400–800 nm (see left part of Figure 4).

Complexes 3–5 revealed similar behaviour under variable-temperature UV-visible (UV-vis.) measurements. At lower temperatures, a broad adsorption band with a λ_{\max} = ca. 534 nm (3) or ca. 540 nm (4, 5) occurred, typical of the ¹A₁ → ¹T₁ transition for Fe(II) complexes in the LS state [28]. As the temperature increased, the absorbance of this band decreased to reach a minimum value at ca. 343 K, which was the highest temperature available with our setup. The conversion of each complex into the HS state is shown by the plot of maximum absorbance at 534 nm (3) or 540 nm (4, 5), as a function of temperature (see right part of Figure 4). These data were used to extract thermodynamic parameters for the SCO process by fitting them to Equation (1) (the ideal solution model derived to fit the data assuming the van't Hoff equation and the Beer-Lambert law [29]), where *A* = Absorbance; *A*_{HS} = Absorbance at HS; *A*_{LS} = Absorbance at LS; ΔH and ΔS are the enthalpy and entropy of the SCO process, respectively; *T* = temperature; *T*_{1/2} = temperature at which concentrations of HS and LS states are equal to 50% with $T_{1/2} = \Delta H/\Delta S$.

$$A = A_{LS} - \frac{A_{LS} - A_{HS}}{\left(1 + \exp\left(\frac{\Delta H}{R} \left(\frac{1}{T} - \frac{1}{T_{1/2}}\right)\right)\right)} \quad (1)$$

Thermodynamic parameters ΔH , ΔS and *T*_{1/2} values have been derived for each of the complexes 3–5 and are listed in Table 2. The values determined for the thermodynamic parameters for complexes 3–5 fall within the range of those reported for similar compounds, comprising a similar coordination sphere and exhibiting solution-phase SCO process [30,31].

Table 2. Summary of SCO data for compounds 1–5.

	Magnetic Behaviour	<i>T</i> _{1/2} (K)	ΔS (J K ⁻¹ mol ⁻¹)	ΔH (kJ mol ⁻¹)
1	LS	-	-	-
2	LS	-	-	-
3	SCO	299.5 (±0.4)	237 (±8)	71 (±2)
4	SCO	290 (±2)	131 (±7)	38 (±2)
5	SCO	299.0 (±0.4)	158 (±4)	47 (±1)

Concentrations of acetonitrile solutions are as follows: [3] = 0.40 mmol L⁻¹; [4] = 0.24 mmol L⁻¹; [5] = 0.25 mmol L⁻¹, measured between the temperature range 275 or 283–343 K and 400–800 nm.

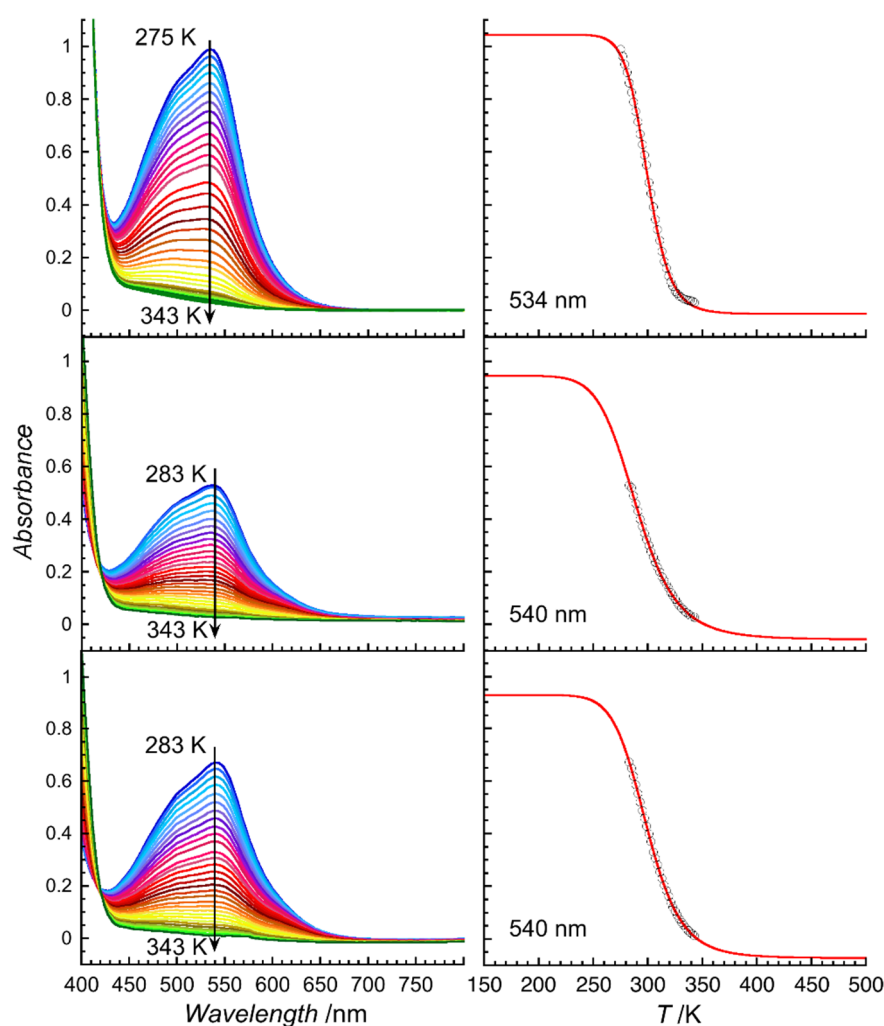


Figure 4. Temperature dependence of the UV-visible (UV-Vis.) spectra between 400–800 nm (left) and of the maximum absorption (right) at 534 nm (complex 3, top) and 540 nm (complex 4, middle, and complex 5, bottom) in acetonitrile solution.

3. Discussion

3.1. Single Crystal Structures

In this study, a series of mononuclear Fe(II) complexes with electron-withdrawing substituents were synthesised. Interestingly, although attempts were made to preferentially form the *tris*-coordinated species, $[\text{Fe}(\text{L})_3](\text{BF}_4)_2$, all five of the complexes studied within this series crystallised as the *bis*-form with two coordinating acetonitrile molecules. We speculate that the poor σ -donating ability of the imine N-donor was a potential cause for preferred coordination of NCCH_3 , and not steric congestion about the Fe(II) node; literature reports of a $[\text{Fe}(\text{L})_2(\text{NCCH}_3)_2]$ analogue, where X = H and Y = H, support this [32,33]. As described in the structural section, an apparent phase transition was observed below 220 K, which at this stage is not understood for complexes 3–5. The metastable state, which readily crystallises at room temperature, underwent significant alterations within the crystal lattice resulting in rapid degradation of the crystal when cooled below ca. 220 K. It is difficult to understand why this degradation only occurred in complexes 3–5 and not in 1–2. Unfortunately, a survey of structural differences between these two sets of complexes, providing some insight into this, was hindered based on the different collection temperature structures that were measured.

3.2. VT-UV-Visible Measurements for Characterisation of SCO

The over-arching aim of this study was to investigate the influence of electron-withdrawing groups and their contribution to electronic and ligand field effects within SCO complexes. As such, a series of complexes were formed, based on the variation of substituents at two locations (shown as “X” and “Y” in Figure 1) on 2-pyridylimine-based ligands. Substitution of “X” variants follows an increasing trend in electronegative character, based on Hammett potentials [34] CF_3 (+0.54) < CN (+0.66) < NO_2 (+0.778), producing complexes 1, 2 and 3, respectively; while substitution of “Y” variants (when X = NO_2) follows a trend in electronegative character, based on Hammett potentials Cl (+0.373) < Br (+0.393), producing complexes 4 and 5, respectively.

Solution-state assessment of complexes 1–5 revealed complexes incorporating ligands with more highly electronegative substituents (complexes 3–5) underwent a colour change in the solution when heated, indicative of SCO. Based on this, it became apparent that the nature of the X substituent was influential in modifying the σ -donor and π -acceptor ability of the N-donor atoms. For example, the stronger electron-withdrawing nature of the NO_2 was able to de-activate the phenyl-group (producing a weaker σ -donor of the N-imine), leaving an overall weaker ligand field in their coordinated complexes.

Further variable-temperature UV-vis. spectroscopic studies were performed on complexes 3–5 to probe the influence of “Y” on SCO. Thermodynamic parameters (ΔS and ΔH) and $T_{1/2}$ values were calculated following fitting of the data to Equation (1); however, as shown in Table 2, the identity of “Y” bore little influence on these. We speculate the minimal influence of Y upon SCO was a consequence of the ring position relative to the pyridyl N-donor (meta- rather than para-position).

While our family of complexes showed a trend towards stabilization of the HS state with increased electronegativity at X, notably Halcrow et al. [23] have recently reported that there is conflicting evidence of whether added electronegativity stabilises the HS state [24,35] or the LS state [22,36–39]. They report that the addition of electron-withdrawing substituents to ligands stabilises either the LS or the HS state depending on their position in the molecule and on which types of substituents are considered. Solid-state DC magnetic susceptibility studies were not performed to further probe the SCO of complexes 3–5 as the detection of a phase transition from the single crystal data with cooling and the likely loss of coordinated solvent with heating precluded the study of the solid material. Furthermore, performing SCO studies exclusively in the solution-state for complexes 3–5 overcomes the introduction of further supramolecular influences in the crystal lattice, which might confuse the interpretation of the influence of electron-withdrawing groups on coordinated ligands.

The determination of ligand exchange or solvolysis processes can be identified based on the magnitude of the thermodynamic parameters of complexes in the solution. The thermodynamic parameters for complexes 3–5 (see Table 2) fall broadly in line with the expected values for potential ligand exchange. We can compare our results to an example by Bryliakov which showed thermodynamic parameters of ca. $\Delta H = 40 \text{ kJ mol}^{-1}$ and ca. $\Delta S = 137 \text{ J mol}^{-1}$ for the dissociation of one acetonitrile molecule from the complex $[\text{Fe}(\text{BPMEN})(\text{CH}_3\text{CN})_2](\text{ClO}_4)_2$ [40]. Further investigation is necessary to precisely determine the potential for ligand exchange within complexes 3–5 in the solution.

3.3. Conclusions

A family of Fe(II) compounds of formula *cis*- $[\text{Fe}(\text{L})_2(\text{CH}_3\text{CN})_2](\text{BF}_4)_2 \cdot x\text{CH}_3\text{CN}$ are reported on here. Variations of electron withdrawing groups at two positions on 2-pyridylimine-based ligands were investigated in terms of their ability to tune the SCO of their Fe(II) complexes. VT-solution-state studies revealed that complexes incorporating stronger electron-withdrawing groups at position X (e.g., NO_2) were able to undergo SCO (compared to the parent LS complex) due to a weakening of the ligand field. Variations of substituents at position Y (when X = NO_2) were insufficient in altering the SCO and $T_{1/2}$ of their complexes, likely based on their position in the ligand, meta to the pyridyl N-donor. These results serve to emphasise the advantages offered by the tunability of SCO compounds and provide design strategies for establishing new variants. Current work in our laboratory is looking

at new variants of compounds 1–5 by using related ligand sets and results from these studies will be reported in due course.

4. Materials and Methods

Unless otherwise specified, all reagents and starting materials were reagent grade, purchased from standard suppliers and used as received. Elemental analyses were carried out by Campbell Microanalytical Laboratory, University of Otago, New Zealand. Infrared spectra were recorded either on a Perkin-Elmer Spectrum One FTIR instrument operating in diffuse reflectance mode with samples prepared as KBr mulls (KBr), or on a Perkin Elmer Spectrum 100 spectrometer with Universal ATR accessory over the range of 4000–650 cm^{-1} . The following abbreviations are used, vs: very strong, s: strong, m: medium, w: weak, sh: sharp and br: broad. UV-visible spectra were recorded on a Varian CARY UV-Visible spectrometer in the range 400–800 nm unless otherwise stated. Samples were measured in quartz cuvettes of path length 1 cm and approximate capacity of 3 mL. The concentrations of solutions used were as follows: [3] = 0.4 mmol L^{-1} ; [4] = 0.24 mmol L^{-1} ; [5] = 0.25 mmol L^{-1} . The temperature profile for complexes 3, 4 and 5 followed initial cooling of the samples in the solution to 275 or 283 K, then heating in 2 K increments to 343 K.

Mass spectra were recorded on either a DIONEX Ultimate 3000 or Bruker MaXis 4G spectrometer, both of which were operated in high-resolution positive ion electrospray mode. Samples were dissolved and diluted to the required concentration in appropriate HPLC-grade solvents—generally acetonitrile or methanol.

X-ray crystallographic data collection and refinement were carried out with an Oxford Agilent SuperNova instrument (for complexes 1 and 2) with focused microsource Cu $K\alpha$ ($\lambda = 1.5418 \text{ \AA}$) radiation and an ATLAS CCD area detector or with a Bruker APEX-II instrument (for complexes 3–5), using graphite-monochromated Mo $K\alpha$ ($\lambda = 0.71073 \text{ \AA}$) radiation. All structures were solved using direct methods or charge splitting with SHELXS [41] and refined on F^2 using all data by full matrix least-squares procedures with SHELXL-97 [42] within the program OLEX-2 [43]. Non-hydrogen atoms were refined with anisotropic displacement parameters. Hydrogen atoms were included in calculated positions, or were manually assigned from residual electron density where appropriate. Graphical representations of crystallographic data were prepared using the CrystalMaker, OLEX-2 and Mercury software packages. Crystallographic data for all compounds are included in .cif format as electronic supplementary information. For complexes 2, 4 and 5 the counter anion $[\text{BF}_4]^-$ was found to be disordered and rotated through two positions with occupancies refined at 75:25 for complex 2 and 50:50 for complexes 4 and 5. CCDC numbers correspond to 1891997–1892001 for compounds 1–5.

Synthetic procedures:

N-(pyridin-2-ylmethylene)-4-(trifluoromethyl)aniline—L1

p-trifluoromethylaniline (500 mg, 3.1 mmol) was dissolved in 20 mL of ethanol with gentle heating. A separate suspension of 2-pyridinecarboxaldehyde (332 mg, 3.1 mmol) was prepared in 20 mL of ethanol. The aldehyde suspension was added portion-wise to the stirring 4-trifluoromethylaniline solution and the resultant mixture refluxed for 3 h. Then the solution was cooled to room temperature and the solvent removed in vacuo to give a yellow oily product. Attempts to purify the product were unsuccessful and, as such, it was used in its crude form for complexation. IR (ATR, cm^{-1}) 3343 br, 1614 s, 1534 s, 1474 m, 1438 m, 1316 m, 1160 m, 1097 s, 1061 s, 985 s, 886 w, 828 s, 757 s, 675 s, 588 m.

4-((pyridin-2-ylmethylene)amino)benzotrile—L2

p-Aminobenzotrile (310 mg, 2.6 mmol) and pyridine-2-carboxaldehyde (280 mg, 2.6 mmol) were dissolved in 20 mL of methanol. The reaction mixture was heated at reflux for 3 h and the resulting yellow solution was cooled to room temperature. The excess solvent was removed in vacuo to give a yellow residue. The residue was then dissolved in 10 mL of dichloromethane and was dried over anhydrous MgSO_4 and the excess solvent removed again in vacuo to give the product as a yellow

oil. Attempts to purify the product were unsuccessful and, as such, it was used in its crude form for complexation. m/z (ESMS) 208.0868 [M + H⁺] calculated for C₁₃H₁₀N₃ 208.0869; IR (KBr, cm⁻¹) 3317 m, 2216 m, 1593 s, 1518 m, 1436 m, 1422 m, 1320 m, 1093 m, 1051 m, 1015 m, 991 s, 828 m, 780 m, 753 m, 625 m, 613 m, 535 m.

4-nitro-N-(pyridin-2-ylmethylene)aniline—L3

p-nitroaniline (2 g, 14.5 mmol) was dissolved in ethanol (40 mL) and heated at reflux until all solids dissolved. 2-Pyridinecarboxaldehyde (1.4 mL, 14.5 mmol) was added followed by several drops of glacial acetic acid. The resulting yellow solution was heated at reflux for two hours followed by cooling to room temperature. The solvent was removed under reduced pressure and the resulting brown oil was dried under high vacuum at 50 °C until an orange solid formed. The solid was slurried in petroleum ether and filtered to give a pale-yellow solid. Yield: 2.99 g (91%); ¹H-NMR: (CDCl₃) 10.08 (s, 1 H), 8.79 (d, J = 4.20, 1 H), 8.06 (d, J = 7.50, 2 H), 7.97 (d, J = 7.80, 1 H), 7.88 (t, J = 7.80, 1 H), 7.53 (m, 1 H), 6.61 (d, J = 7.50, 2 H); IR (KBr, cm⁻¹) 1595 m, 1552 m, 1525 m, 1307 m, 1181 m, 1132 m, 1123 m, 1001 m, 906 m, 840 m, 828 m, 775 m, 751 m, 723 m, 694 m.

[Fe(L1)₂(CH₃CN)₂](BF₄)₂·2CH₃CN—complex 1

L1 (50 mg, 0.2 mmol) was suspended in 10 mL of acetonitrile. To this suspension was added Fe(BF₄)₂·6H₂O (33 mg, 0.1 mmol). The resulting red solution was mildly heated and stirred for 1 h and left to cool to room temperature. The reaction solution was filtered. The filtrate was placed in a small vial inside a larger vessel containing diethyl ether, which diffused into the complex solution over time. Red block crystals suitable for single crystal X-ray diffraction formed after two weeks. Yield: 15 mg (16%); found: C 42.8, H 3.2, N 10.4, C₃₀H₂₄B₂N₆F₁₄Fe·2H₂O (1 – 2CH₃CN + 2H₂O) requires: C 42.5, H 3.3, N 9.9; IR (ATR, cm⁻¹) 3032 w, 1608 m, 1586 m, 1471 m, 1442 m, 1319 s, 1166 s, 1051 a, 847 s, 768 s, 660 s, 609 s.

[Fe(L2)₂(CH₃CN)₂](BF₄)₂·2CH₃CN—complex 2

L2 (20 mg, 0.10 mmol) and Fe(BF₄)₂·6H₂O (20 mg, 0.05 mmol) were mixed in 1 mL of acetonitrile. The resulting purple solution was carefully layered with 2 mL of diethyl ether and left to stand in the freezer for two days. After this time dark purple block crystals suitable for single crystal X-ray diffraction formed. Yield: 10 mg (24%); unable to obtain sufficient crystalline sample for microanalysis; IR (ATR cm⁻¹) 3518 br, 2232 s, 1600 s, 1499 m, 1444 m, 1204 m, 1065 br s, 852 m, 786 m, 568 m, 523 s, 502 m, 463 m.

[Fe(L3)₂(CH₃CN)₂](BF₄)₂—complex 3

L3 (50 mg, 0.22 mmol) was suspended in 5 mL of acetonitrile. To this solution Fe(BF₄)₂·6H₂O (45 mg, 0.12 mmol) was added resulting in the formation of a raspberry red solution. The reaction mixture was carefully layered with approximately 3 mL of diethyl ether and left to stand for a few days. After this time the product formed as black block crystals. Yield: 51 mg (55%); found: C 42.8, H 2.9, N 13.5, C₂₆H₂₁B₂F₈FeN₇O₄ (3 – 1CH₃CN) requires: C 43.08, H 2.92, N 13.52; UV-Vis. (ε) 534 nm (2120 L mol⁻¹ cm⁻¹); IR (ATR, cm⁻¹) 3504 br, 1624 m, 1588 m, 1486 m, 1447 w, 1346 s, 1312 w, 1198 w, 1166 w, 1026 br s, 1006 br s, 912 m, 855 m, 779 m, 743 m, 701 m, 689 m, 546 m, 522 m, 455 m.

[Fe(L4)₂(CH₃CN)₂](BF₄)₂—complex 4

5-chloro-2-pyridinecarboxaldehyde (31 mg, 0.22 mmol) and *p*-nitroaniline (30 mg, 0.22 mmol) were stirred in acetonitrile (3 mL) at 50 °C for 3 h to give a yellow solution. A solution of Fe(BF₄)₂·6H₂O (37 mg, 0.11 mmol) in acetonitrile (3 mL) was added and the resulting red solution stirred at 50 °C for 3 h. After cooling to room temperature, the solution was filtered and vapor diffusion of diethyl ether gave dark red/purple block crystals suitable for single crystal X-ray diffraction. Yield: 24 mg (26%); found: C 39.8, H 2.4, N 13.0, C₂₈H₂₂Cl₂B₂F₈Fe₁N₈O₄ requires C 40.28, H 2.66, N 13.42; UV-Vis.

(ϵ) 540 nm (2180 L mol⁻¹ cm⁻¹); IR (ATR, cm⁻¹) 3398 br, 1589 s, 1552 s, 1519 s, 1484 s, 1346 s, 1305 s, 1195 m, 1037 br, 914 s, 856 s, 757 s, 734 s, 692 s.

[Fe(L5)₂(CH₃CN)₂](BF₄)₂—complex 5

5-bromo-2-pyridinecarboxaldehyde (41 mg, 0.22 mmol) and *p*-nitroaniline (30 mg, 0.22 mmol) were stirred in acetonitrile (3 mL) at 50 °C for 3 h to give a yellow solution. A solution of Fe(BF₄)₂·6H₂O (37 mg, 0.11 mmol) in acetonitrile (3 mL) was added and the resulting red solution stirred at 50 °C for 3 h. After cooling to room temperature, the solution was filtered and vapour diffusion of diethyl ether gave dark red/purple block crystals suitable for single crystal X-ray diffraction. Yield: 31 mg (30%); found: C 35.9, H 2.4, N 12.0, C₂₈H₂₂Br₂B₂F₈Fe₁N₈O₄ requires C 36.40, H 2.40, N 12.13; UV-Vis. (ϵ) 540 nm (2670 L mol⁻¹ cm⁻¹); IR (ATR, cm⁻¹) 3446 s, 3108 m, 1608 s, 1589 s, 1546 s, 1521 s, 1346 s, 1199 s, 1095 s, 1027 s, 914 s, 860 s, 757 s, 721 s, 692 s, 655 m.

Supplementary Materials: These are available online at <http://www.mdpi.com/2312-7481/5/2/22/s1>. Table S1. Crystallographic data for 1–5; Table S2. Selected coordination bond angles for 1–5; Table S3. Selected coordination bond lengths for 1–5; Table S4. Inter- and intra-molecular interactions and close contacts in 1–5; Figure S1. Labelled asymmetric unit of 1; Figure S2. Labelled asymmetric unit of 2; Figure S3. Labelled asymmetric unit of 3; Figure S4. Labelled asymmetric unit of 4; Figure S5. Labelled asymmetric unit of 5; Figure S6. Packing diagrams, shown with a view down the b-axis. (a). Complex 1 (isostructural and same collection temperature, 120 K, as 2); (b). Complex 3 at 293 K; (c). Complex 4 (isostructural and same collection temperature, 270 K, as 5). Unit cell shown in red; Figure S7. Packing diagrams, shown with a view down the c-axis. (a). Complex 1 (isostructural and same collection temperature, 120 K, as 2); (b). Complex 3 at 293 K; (c). Complex 4 (isostructural and same collection temperature, 270 K, as 5). Unit cell shown in red, and Variable Temperature UV-vis. Measurements on Complexes 3–5.

Author Contributions: Project conceptualisation by P.E.K., R.J.A.; synthesis by R.J.A., H.S.S., B.H.W.; X-ray characterisation by R.J.A., B.H.W., H.S.S.; VT-UV-Vis. experiments performed and analysed by B.H.W., R.J.A., R.C., C.M.; project supervision by P.E.K., R.C., C.M.; manuscript prepared and edited by H.S.S., R.C., P.E.K.

Funding: This research was funded by the MacDiarmid Institute and the Royal Society of New Zealand Marsden Fund, the Dumont d’Urville NZ-France Science & Technology Support Programme (DDU-UOC1401, N°34176ZJ) and the New Zealand France Friendship Fund. The University of Bordeaux, the CNRS, the Région Nouvelle Aquitaine, the MOLSPIN COST action CA15128 and the GdR MCM-2: Magnétisme et Commutation Moléculaires are also thanked for their financial support.

Acknowledgments: The authors gratefully acknowledge the MacDiarmid Institute and the Royal Society of New Zealand Marsden Fund, the Dumont d’Urville NZ-France Science & Technology Support Programme for financial support (DDU-UOC1401, N°34176ZJ) and the New Zealand France Friendship Fund for the award of an Excellence Scholarship to B.H.W. The University of Bordeaux, the CNRS, the Région Nouvelle Aquitaine, the MOLSPIN COST action CA15128 and the GdR MCM-2: Magnétisme et Commutation Moléculaires are also thanked for their financial support. B.H.W. gratefully acknowledges the University of Canterbury for the receipt of the Roper Scholarship (UC).

Conflicts of Interest: The authors declare no conflict of interest.

References

1. Gütllich, P.; Goodwin, H.A. Spin-crossover in Transition metal compounds. In *Topics in Current Chemistry*; Springer: Berlin, Germany, 2004.
2. Halcrow, M.A. Spin Crossover Materials. In *Properties and Applications*; Wiley: London, UK, 2013.
3. Bousseksou, A.; Molnar, G.; Salmon, L.; Nicolazzi, W. Molecular spin crossover phenomenon: Recent achievements and prospects. *Chem. Soc. Rev.* **2011**, *40*, 3313–3335. [[CrossRef](#)]
4. Kahn, O.; Martinez, C.J. Spin-Transition Polymers: From Molecular Materials Toward Memory Devices. *Science* **1998**, *279*, 44–48. [[CrossRef](#)]
5. Gentili, D.; Demitri, N.; Schafer, B.; Liscio, F.; Bergenti, I.; Ruani, G.; Ruben, M.; Cavallini, M. Multi-modal sensing in spin crossover compounds. *J. Mater. Chem. C* **2015**, *3*, 7836–7844. [[CrossRef](#)]
6. Prins, F.; Monrabal-Capilla, M.; Osorio, E.A.; Coronado, E.; van der Zant, H.S.J. Room-Temperature Electrical Addressing of a Bistable Spin-Crossover Molecular System. *Adv. Mater.* **2011**, *23*, 1545–1549. [[CrossRef](#)]
7. Gütllich, P.; Garcia, Y.; Goodwin, H.A. Spin crossover phenomena in Fe(II) complexes. *Chem. Soc. Rev.* **2000**, *29*, 419–427. [[CrossRef](#)]

8. Gütlich, P.; Gaspar, A.B.; Garcia, Y. Spin state switching in iron coordination compounds. *Beilstein J. Org. Chem.* **2013**, *9*, 342–391. [[CrossRef](#)]
9. Pinkowicz, D.; Rams, M.; Misek, M.; Kamenev, K.V.; Tomkowiak, H.; Katrusiak, A.; Sieklucka, B. Enforcing multifunctionality: A pressure-induced spin-crossover photomagnet. *J. Am. Chem. Soc.* **2015**, *137*, 8795–8802. [[CrossRef](#)] [[PubMed](#)]
10. Gütlich, P.; Ksenofontov, V.; Gaspar, A.B. Pressure effect studies on spin crossover systems. *Coord. Chem. Rev.* **2005**, *249*, 1811–1829. [[CrossRef](#)]
11. Ohkoshi, S.-I.; Imoto, K.; Tsunobuchi, Y.; Takano, S.; Tokoro, H. Light-induced spin-crossover magnet. *Nat. Chem.* **2011**, *3*, 564–569. [[CrossRef](#)] [[PubMed](#)]
12. Halcrow, M.A. Spin-crossover compounds with wide thermal hysteresis. *Chem. Lett.* **2014**, *43*, 1178–1188. [[CrossRef](#)]
13. Hauser, A. Ligand Field Theoretical Considerations, Spin Crossover in Transition Metal Compounds I. *Top. Curr. Chem.* **2004**, *233*, 49–58. [[CrossRef](#)]
14. Murray, K.S.; Kepert, C.J. Cooperativity in spin crossover systems: Memory, magnetism and microporosity. In *Spin Crossover in Transition Metal Compounds I*; Springer: Berlin/Heidelberg, Germany, 2004; Volume 233, pp. 195–228. [[CrossRef](#)]
15. Scott, H.S.; Ross, T.M.; Phonsri, W.; Moubaraki, B.; Chastanet, G.; Létard, J.-F.; Batten, S.R.; Murray, K.S. Discrete Fe^{II} Spin-Crossover Complexes of 2,2'-Dipyridylamino-Substituted s-Triazine Ligands with Phenoxo, Cyanophenoxo and Dibenzylamino Functionalities. *Eur. J. Inorg. Chem.* **2015**, *2015*, 763–777. [[CrossRef](#)]
16. Ross, T.M.; Moubaraki, B.; Neville, S.M.; Batten, S.R.; Murray, K.S. Polymorphism and spin crossover in mononuclear Fe^{II} species containing new dipyridylamino-substituted s-triazine ligands. *Dalton Trans.* **2012**, *41*, 1512–1523. [[CrossRef](#)] [[PubMed](#)]
17. Phonsri, W.; Harding, D.J.; Harding, P.; Murray, K.S.; Moubaraki, B.; Gass, I.A.; Cashion, J.D.; Jameson, G.N.L.; Adams, H. Stepped spin crossover in Fe(III) halogen substituted quinolylsalicylaldimine complexes. *Dalton Trans.* **2014**, *43*, 17509–17518. [[CrossRef](#)]
18. Scott, H.S.; Stanilands, R.W.; Kruger, P.E. Spin crossover in homoleptic Fe(II) imidazolylimine complexes. *Coord. Chem. Rev.* **2018**, *362*, 24–43. [[CrossRef](#)]
19. Weber, B.; Walker, F.A. Solution NMR Studies of Iron(II) Spin-Crossover Complexes. *Inorg. Chem.* **2007**, *46*, 6794–6803. [[CrossRef](#)] [[PubMed](#)]
20. Archer, R.J.; Scott, H.S.; Polson, M.I.J.; Williamson, B.E.; Mathonière, C.; Rouzières, M.; Clérac, R.; Kruger, P.E. Varied spin crossover behaviour in a family of dinuclear Fe(II) triple helicate complexes. *Dalton Trans.* **2018**, *47*, 7965–7974. [[CrossRef](#)]
21. Wei, H.-H.; Hsiao, C.-S. Synthesis and Mössbauer Spectroscopy Studies on the Spin States of tris(2-Pyridylimine) Iron(ii) Complexes. *J. Chin. Chem. Soc.* **1981**, *28*, 69–73. [[CrossRef](#)]
22. Nakano, K.; Suemura, N.; Yoneda, K.; Kawata, S.; Kaizaki, S. Substituent effect of the coordinated pyridine in a series of pyrazolato bridged dinuclear diiron(II) complexes on the spin-crossover behaviour. *Dalton Trans.* **2005**, *4*, 740–743. [[CrossRef](#)]
23. Cook, L.J.K.; Kulmaczewski, R.; Mohammed, R.; Dudley, S.; Barrett, S.A.; Little, M.A.; Deeth, R.J.; Halcrow, M.A. A Unified Treatment of the Relationship Between Ligand Substituents and Spin State in a Family of Iron(II) Complexes. *Angew. Chem. Int. Ed.* **2016**, *55*, 4327–4331. [[CrossRef](#)]
24. Park, J.G.; Jeon, I.-R.; Harris, T.D. Electronic Effects of Ligand Substitution on Spin Crossover in a Series of Diiminoquinonoid-Bridged Fe^{II}₂ Complexes. *Inorg. Chem.* **2015**, *54*, 359–369. [[CrossRef](#)]
25. Zhang, J.; Campolo, D.; Dumur, F.; Xiao, P.; Fouassier, J.P.; Gignes, D.; Lalevee, J. Iron complexes as photoinitiators for radical and cationic polymerization through photoredox catalysis processes. *J. Polym. Sci. A* **2015**, *53*, 42–49. [[CrossRef](#)]
26. Guionneau, P.; Marchivie, M.; Bravic, G.; Létard, J.-F.; Chasseau, D. Structural Aspects of Spin Crossover. Example of the [Fe^{II}L_n(NCS)₂] Complexes. *Top. Curr. Chem.* **2004**, *234*, 97–128. [[CrossRef](#)]
27. Janiak, C. A critical account on π–π stacking in metal complexes with aromatic nitrogen-containing ligands. *J. Chem. Soc. Dalton Trans.* **2000**, 3885–3896. [[CrossRef](#)]
28. Hauser, A. Light Induced Spin Crossover and the High Spin to Low Spin Relaxation. *Top. Curr. Chem.* **2004**, *234*, 155–198. [[CrossRef](#)]
29. Atkins, P.; Paula, J.D. *Physical Chemistry*; Oxford University Press: Oxford, UK, 2006.

30. Toftlund, H. Spin equilibria in iron(II) complexes. *Coord. Chem. Rev.* **1989**, *94*, 67–108. [[CrossRef](#)]
31. McGarvey, J.J.; Lawthers, I.; Heremans, K.; Toftlund, H. Spin-state relaxation dynamics in iron(II) complexes: Solvent on the activation and reaction and volumes for the 1A \rightleftharpoons 5T interconversion. *J. Chem. Soc. Chem. Commun.* **1984**, *23*, 1575–1576. [[CrossRef](#)]
32. Martínez-Ferraté, O.; Britovsek, G.J.P.; Claver, C.; van Leeuwen, P.W.N.M. C–H benzylic oxidation promoted by dinuclear iron DBDOC iminopyridine complexes. *Inorg. Chim. Acta* **2015**, *431*, 156–160. [[CrossRef](#)]
33. Martínez-Ferraté, O. Synthesis of Dinuclear Complexes. From Ligand Design to Catalysis. Ph.D. Thesis, Universitat Rovira i Virgili, Tarragona, Spain, 2013.
34. Hansch, C.; Leo, A.; Taft, R.W. A survey of Hammett substituent constants and resonance and field parameters. *Chem. Rev.* **1991**, *91*, 165–195. [[CrossRef](#)]
35. Lin, H.-J.; Siretanu, D.; Dickie, D.A.; Subedi, D.; Scepaniak, J.J.; Mitcov, D.; Clérac, R.; Smith, J.M. Steric and Electronic Control of the Spin State in Three-Fold Symmetric, Four-Coordinate Iron(II) Complexes. *J. Am. Chem. Soc.* **2014**, *136*, 13326–13332. [[CrossRef](#)] [[PubMed](#)]
36. Tweedle, M.F.; Wilson, L.J. Variable spin iron(III) chelates with hexadentate ligands derived from triethylenetetramine and various salicylaldehydes. Synthesis, characterization, and solution state studies of a new 2T. d_{blarw}. 6A spin equilibrium system. *J. Am. Chem. Soc.* **1976**, *98*, 4824–4834. [[CrossRef](#)]
37. Prat, I.; Company, A.; Corona, T.; Parella, T.; Ribas, X.; Costas, M. Assessing the Impact of Electronic and Steric Tuning of the Ligand in the Spin State and Catalytic Oxidation Ability of the Fe^{II}(Pytacn) Family of Complexes. *Inorg. Chem.* **2013**, *52*, 9229–9244. [[CrossRef](#)] [[PubMed](#)]
38. Houghton, J.; Deeth, R.J. Spin-State Energetics of Fe^{II} Complexes—The Continuing Voyage Through the Density Functional Minefield. *Eur. J. Inorg. Chem.* **2014**, *2014*, 4573–4580. [[CrossRef](#)]
39. Takahashi, K.; Hasegawa, Y.; Sakamoto, R.; Nishikawa, M.; Kume, S.; Nishibori, E.; Nishihara, H. Solid-State Ligand-Driven Light-Induced Spin Change at Ambient Temperatures in Bis(dipyrazolylstyrylpyridine)iron(II) Complexes. *Inorg. Chem.* **2012**, *51*, 5188–5198. [[CrossRef](#)] [[PubMed](#)]
40. Bryliakov, K.P.; Duban, E.A.; Talsi, E.P. The Nature of the Spin-State Variation of [FeII(BPMEN)(CH₃CN)₂](ClO₄)₂ in Solution. *Eur. J. Inorg. Chem.* **2005**, *72*–76. [[CrossRef](#)]
41. Sheldrick, G.M. A short history of SHELX. *Acta Crystallogr. Sect. A Found. Crystallogr.* **2008**, *64*, 112–122. [[CrossRef](#)] [[PubMed](#)]
42. Sheldrick, G.M. *SHELXL-97, Programs for X-ray Crystal Structure Refinement*; University of Gottingen: Gottingen, Germany, 1997.
43. Dolomanov, O.V.; Bourhis, L.J.; Gildea, R.J.; Howard, J.A.K.; Puschmann, H. OLEX2: A complete structure solution, refinement and analysis program. *J. Appl. Crystallogr.* **2009**, *42*, 339–341. [[CrossRef](#)]



© 2019 by the authors. Licensee MDPI, Basel, Switzerland. This article is an open access article distributed under the terms and conditions of the Creative Commons Attribution (CC BY) license (<http://creativecommons.org/licenses/by/4.0/>).